Finally, uniform alignment of the axis of easy magnetization, ultra fine grains, and an increase in the degree of ordering are needed to achieve higher energy product and coercivity. Both alloy chemistry and processing techniques limit the development of these features.

V. Conclusion

Extruded Mn-Al-C magnets are fine grained, heavily twinned, and contain a high density of dislocations and a dispersion of Al_2O_3. Although some grains are disordered, no anti-phase boundaries have been detected in the ordered $L1_0$ grains.

The effect of Ni addition on the structure-magnetic properties relation is established as follows: nickel helps in the development of magnetic anisotropy during the deformation process resulting in uniformly fine grains and a high density of twins. Atomistically, nickel atoms couple ferromagnetically with manganese atoms changing the local Mn atomic environment. All these account for the higher H_c and $(BH)_{max}$ values for the Ni-containing Mn-Al-C magnet.

Acknowledgment

The authors wish to thank the Matsushita Electric Industrial Company of Japan for supplying the material used in this study. Helpful discussions with Y. Sakamoto are acknowledged.

References

[1] W. Owa, T. Mukakami, Y. Kondo, T. Otani, S. Kojima, and Y. Sakamoto, National Tech. Rep. 26, pp. 826-836, Oct. 1980.
[2] T. Ohtani, N. Katop, S. Kojima, K. Kojima, Y. Sakamoto, I. Konno, M. Tsukahara, and T. Kubo, "Magnetic properties of Mn-Al-C permanent magnet alloys," *IEEE Trans. Magn.*, vol. MAG-13, pp. 1328-1330, Sep. 1977.
[3] M. A. Bohlman, J. C. Koo, and J. H. Wise, *J. Appl. Phys.*, vol. 52, pp. 2542-2543, 1981.
[4] S. Kojima, T. Ohtani, N. Kato, K. Kojima, Y. Sakamoto, I. Konno, M. Tsukahara, and T. Kubo, *AIP Conf. Proc.*, vol. 24, pp. 768-769, 1974.
[5] J. J. Van den Broek, H. Donkersloot, G. Van Tendeloo, and J. Van Landuyt, *Acta Met.*, vol. 27, pp. 1497-1504, 1979.
[6] R. Rothwarf, H. Leupold, J. T. Breslin, A. Tauber, and D. I. Paul, *J. Appl. Phys.*, vol. 52, pp. 2515-2516, 1981.
[7] S. Kojima, K. Kojima, S. Mitani, and T. Kubo, Synopsis of the 1978 Autumn Meeting of the Japanese Institute of Metals, 1978.
[8] J. P. Jakubovics, A. J. Lapworth, and T. W. Jolly, *J. Appl. Phys.*, vol. 49, pp. 2002-2006, 1978.
[9] J. S. Gau, R. Mishra, and G. Thomas, "Precipitates and fracture studies of Mn-Al-C alloys," presented at Annual Meeting of AIME, Atlanta, GA, Mar. 6-10, 1983.
[10] J. V. Landuyt, G. V. Tendeloo, J. J. v.d. Broek, H. Donkersloot, and H. Zijlstra, "Defect structure and magnetic properties of MnAl permanent magnet materials," *IEEE Trans. Magn.*, vol. Mag-14, pp. 679-681, Sep. 1978.
[11] Y. Sakamoto, S. Kojima, K. Kojima, T. Ohtani, and T. Kubo, *J. Appl. Phys.*, vol. 50, pp. 2355-2357, 1979.
[12] B. D. Cullity, *Introduction to Magnetic Materials.* Reading, MA: Addison-Wesley, 1979, ch. 10.
[13] P. B. Hirsh, A. Howie, R. B. Nicholson, D. W. Pashley, and M. J. Whelan, *Electron Microscopy of Thin Crystals.* New York: Kriegar, 1977, ch. 15.
[14] M. J. Marcinkowski, *Electron Microscopy and Strength of Crystals*, G. Thomas and J. Washburn, Eds. London: Interscience, 1963, p. 431.
[15] J. H. Wernick, *Treatise on Solid State Chemistry*, N. B. Hannay, Ed. New York: Plenum, 1973, vol. 1, ch. 4.
[16] G. K. Wertheim and J. H. Wernick, *Acta Met.*, vol. 15, p. 297 1967.
[17] C. G. Shull and M. K. Wilkinson, *Phys. Rev.*, vol. 97, p. 304, 1955.

3-D Finite Element Predictions of Magnetostatic Leakage Fields

NATHAN IDA AND WILLIAM LORD, SENIOR MEMBER, IEEE

Abstract—Traditionally electromagnetic leakage fields have largely been of interest to the designers of electrical machinery and magnetic tape heads. An increasingly important application of such leakage fields, however, relates to their use as a mechanism for the detection of defects in ferromagnetic materials. The finite element simulation of three-dimensional active leakage fields is described, and the theoretical predictions are compared with experimentally obtained leakage field profiles for a rectangular slot in a carbon steel bar. Particular emphasis is placed on techniques for determining boundary conditions and the appropriate excitation current distribution in the bar.

Manuscript received January 17, 1983; revised April 25, 1983. This work was supported by the Army Research Office and the Electric Power Research Institute.

The authors are with Electrical Engineering Department, Colorado State University, Fort Collins, CO 80523.

Introduction

DEVELOPMENTS in the numerical analysis of low frequency electromagnetic phenomena have largely been driven by the need to study the field distributions in electrical machinery [1]-[3] and large magnet structures for fusion applications [4]. During the past decade, parallel developments have taken place in the modeling of electromagnetic phenomena used for the nondestructive testing (NDT) of critical metal structures in the aerospace, transportation energy, and metals industries where reliability, safety, and product quality considerations are important.

Analytical approaches to the modeling of electromagnetic field/defect interactions have largely been unsuccessful due to

0018-9464/83/0900-2260$01.00

both the awkward boundaries associated with realistic defect shapes and the lack of generality that ensues when making the necessary assumptions needed to obtain tractable analytical solutions [5]. Viable models are needed in order to understand the ways in which fields and defects interact to produce measurable indications, to help in the design of detection probes for diverse applications, to simulate those testing environments which are difficult and/or expensive to replicate in the laboratory and, perhaps most important in many of the critical testing situations facing industries today, to provide training data for automated defect characterization schemes.

To-date, two-dimensional and axisymmetric finite element code has been utilized for the study of active, residual, and eddy current NDT techniques [6].

Under active excitation conditions, a direct current is applied to the ferromagnetic specimen setting up leakage fields around surface and subsurface flaws which can then be detected using any magnetic flux sensitive transducer such as a Hall element, moving coil, magnetic tape head, etc. [7]. Active leakage field profiles have been studied using conventional 2-D magnetostatic finite element code taking into account the nonlinear magnetization characteristics of the test specimen [8]. This work has led to the development of a defect characterization algorithm capable of predicting the equivalent width, depth, and inclination of surface defects in ferromagnetic test specimens [9].

Analytically, such phenomena have largely been modeled using an equivalent dipole approximation [10]. It is interesting to note that the equations derived for the dipole equivalent of a rectangular slot are identical in form to those derived by Karlquist [11] for predicting the leakage field of a magnetic tape head. This paper is concerned with extending the 2-D active leakage field modeling to the more important 3-D case and illustrates the procedure by considering the active leakage field around a rectangular slot in a ferromagnetic bar. Particular emphasis is placed on determining the correct current distribution around the rectangular slot before predicting the corresponding leakage field. In addition the 2-D code is used to determine the approximate problem boundary conditions before running the 3-D code.

Electromagnetic Field Equations

The relevant Maxwell equations, defining the magnetostatic field in a region with impressed current densities are given by

$$\nabla \cdot \bar{B} = 0 \tag{1}$$

$$\nabla \times \bar{H} = \bar{J} \tag{2}$$

along with the constitutive relation

$$\bar{B} = \mu \bar{H}. \tag{3}$$

Introducing the magnetic vector potential $\bar{A}$ as

$$\bar{B} = \nabla \times \bar{A} \tag{4}$$

and by substituting (4) and (3) into (2) the magnetostatic field equation is

$$\nabla \times [\nu(\nabla \times \bar{A})] = \bar{J} \tag{5}$$

where ν is the reluctivity tensor in the three-dimensional volume and $\bar{J}$ is the current density vector. The reluctivity can be assumed to be single valued or different in each spatial direction. Changes in material permeability can be modeled by changing the reluctivity for neighboring elements but within each element ν is assumed to be constant. As the magnetic vector potential $\bar{A}$ in (5) is not uniquely specified by the curl equation (4) one may apply the Coulomb gauge $\nabla \cdot \bar{A} = 0$ explicitly [12]. Although the Coulomb gauge is not enforced explicitly in the present work, the zero divergence of the magnetic vector potential is ensured locally by the choice of isoparametric finite elements and the choice of boundary conditions [13].

Three-Dimensional Finite Element Formulation and Discretization

The finite element method used here is based on a variational formulation equivalent to (5) and the associated boundary conditions. A suitable energy functional can be written as

$$F(\bar{A}) = \int_v \{\tfrac{1}{2}\nu(\nabla \times \bar{A}) \cdot (\nabla \times \bar{A}) - \bar{A} \cdot \bar{J}\}\, dv. \tag{6}$$

The stationary point of this functional is found by taking the first variation with respect to each unknown and equating it to zero

$$\delta F(\bar{A}) = \delta \int_v \{\tfrac{1}{2}\nu(\nabla \times \bar{A}) \cdot (\nabla \times \bar{A}) - \bar{A} \cdot \bar{J}\}\, dv = 0. \tag{7}$$

The volume of interest is now discretized into a number of eight node hexahedral isoparametric elements. The magnetic vector potential is approximated at each node in the volume by a set of shape functions [12] N_i:

$$A = \sum_{i=1}^{k} N_i A_i \tag{8}$$

where k is the number of nodal points in each finite element.

Substituting (8) into the variational expression (7) and taking this variation with respect to each unknown variable in an element, one reaches the standard finite element equation for an element

$$[k]_e \{A\}_e - \{Q\}_e = 0 \tag{9}$$

where $[k]_e$ is a (24 X 24) elemental matrix, $\{A\}_e$ is the (24 X 1) vector of unknowns for the element, and $\{Q\}_e$ is the (24 X 1) source vector for the element. The entries in the elemental matrix and source vector are calculated using an eight point Gaussian quadrature. Each elemental equation is then summed into a global matrix of the form

$$[k]\{A\} - \{Q\} = 0 \tag{10}$$

where $[k]$ is the $[3N \times 3N]$ global matrix, $\{A\}$ is the $(3N \times 1)$ unknown vector, $\{Q\}$ is the $(3N \times 1)$ global source vector, and N is the number of nodal points in the solution region. The next step is the application of the boundary conditions to the global system of equations and solution using Gaussian elimination.

The system of (1) is too large to be stored in a computer's memory for any realistic problem, therefore, a frontal method [14], [15] of assembly and elimination has been adopted, rather than the more common in core, banded solution.

Current Density Distribution

In many magnetostatic applications the current density distribution is either known exactly or can be assumed to have a simple approximate distribution. In calculation of leakage fields around two-dimensional slots the current density has only one component in the z direction and is assumed to be uniform everywhere in the current carrying region [16]. In other cases the current density can be approximated in a simple manner such as flow in current sheets [17].

In the calculation of leakage fields around three-dimensional defects, no simplifying assumptions can be made as the very existence of such fields is a result of the three-dimensional distribution of the currents around the defects. In addition defects have irregular boundaries, making the calculation of three components of the current density vector impossible other than by numerical means. In this work the three-dimensional current distribution is calculated by numerically solving Laplace's equation for the electric scalar potential in the current carrying region.

For a source free region the potential distribution can be calculated from Laplace's equation in three-dimensions, for the electric scalar potential

$$\nabla^2 \phi = 0 \tag{11}$$

provided the correct boundary conditions are known. Within the conducting region, for which the current density distribution is sought the following equation applies

$$\bar{J} = -\sigma \nabla \phi \tag{12}$$

where σ is the conductivity tensor. As for the reluctivity tensor in (5), this can be either single valued in the whole conducting region or differ from element to element and can be different in each spatial direction. In this application σ_x, σ_y, and σ_z are not used explicitly but are assumed to be single valued in the whole conducting region. Equation (11) is solved using a finite element formulation in a form similar to that described above. It is, however, simpler in that the resulting global matrix is symmetric and only one scalar unknown is calculated at each node of the discretized volume. Only the current carrying region need be discretized but within this region the elements must correspond identically to the elements in the same region in the finite element discretization of the whole region. This is important since from (12) the current density components are calculated at the centroid of the element and assumed to be constant throughout each element. When introduced in the finite element solution, the boundary of corresponding current carrying elements must match exactly. This requirement is assured by simply using the same mesh data for both the current distribution and the magnetic vector potential calculations.

The solution of (11) using the finite element method is standard and the only complication that can arise is the specification of the boundary conditions for the electric scalar potential. In the case of a slot in a current carrying bar this is simplified by the fact that away from the slot boundaries the current density is uniform and has only one component (Fig. 1). At these boundaries, the boundary conditions are specified as ϕ_1 and ϕ_2, being set arbitrarily to $\phi = 1\text{V}$ on the plane $z = z_0$ and $\phi = 0\text{V}$ on the plane $z = 0$. From this the distribution of the potential is calculated and an arbitrary electric field intensity distribution is calculated as $\bar{E} = -\nabla\phi$. From this the correct current density is found by normalizing these values with respect to the electric field intensity component in the uniform distribution region and multiplying by the impressed current density

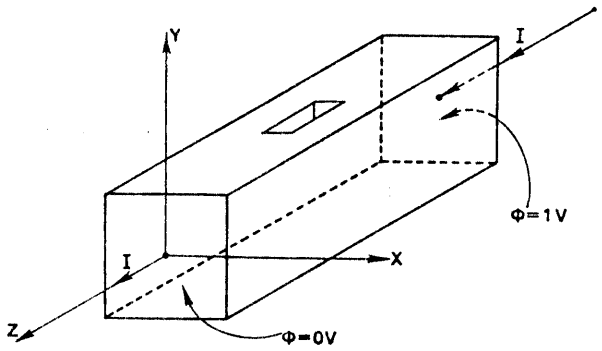

Fig. 1. Bar geometry and boundary conditions for current density calculations.

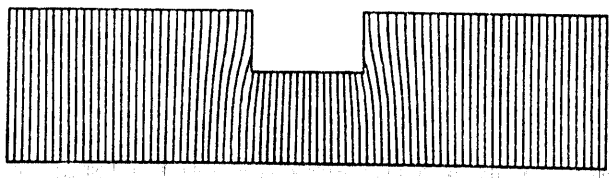

Fig. 2. Constant potential plot on a plane through slot.

$$\bar{J} = \frac{\bar{E}}{E_{z0}} \bar{J}_0 \tag{13}$$

where E_{z0} is the z component of the calculated electric field intensity at the boundary (actually at the centroid of any of the elements in the first layer, at the boundary), and $\bar{J}_0$ is the uniform impressed current density. Both $\bar{E}$ and $\bar{J}_0$ have only a z component at the boundary.

This method avoids both the need to specify exact boundary conditions and the error associated with the specification of the conductivity which is not always known or not known exactly. However, it is implied that the conductivity is single valued everywhere in the conductor and, therefore, spatial variations in σ cannot be accommodated. If this is desired the current densities can be calculated directly from (12).

As the geometry of the bar to be studied is symmetric, only one quadrant of it need be modeled as shown in Fig. 1. Fig. 2 is a plot of constant potential lines at a cross sectional plane through the bar and slot at $x = 0$. The current is normal everywhere to these lines. Table I gives a summary of maximum, minimum, and nominal (uniform) values of current density components. This table clearly shows the importance of current density calculations since large variations in current density exist in the vicinity of the slot. An added benefit of the method described above is that by inspection of potential

TABLE I
MINIMUM, MAXIMUM, AND NOMINAL CURRENT DENSITY COMPONENTS (A/m²)

	Minimum	Maximum	Nominal (Uniform Distribution)
J_x	-3998.27	29 886.9	0
J_y	-22 066.2	1383.53	0
J_z	91 633.0	155 976.4	124 000.0

plots as in Fig. 2 it is possible to decide on the distance away from the slot that the boundaries in the z direction should be placed without having to go through the expensive procedure of boundary perturbation. It also shows that uniform distribution exists very close to the slot boundaries and it is only necessary to discretize a small length of the bar for the 3-D solution.

The current density values are now incorporated in the 3-D finite element procedure as input, along with the mesh and material properties data.

BOUNDARY CONDITIONS

The boundary conditions are specified in terms of the components of the magnetic vector potential. Fig. 3 summarizes these conditions. On the outer boundaries, at $x = x_0$ and $y = y_0$, the components of the magnetic vector potential are set to zero as these are assumed to be remote enough from the bar so as to have negligible flux densities in all three spatial directions. These boundary conditions are applied at a distance 2.5 times larger than the size of the bar, a figure obtained from two-dimensional numerical experiments with a similar problem (identical current density but two-dimensional slot). The boundaries at $x = 0$ and $y = 0$ are symmetry planes, therefore, these are left as open boundaries. At $z = 0$ and $z = z_0$, the impressed current crosses the boundaries and there the boundary conditions are specified explicitly in terms of the components of the magnetic vector potential. As pointed out earlier, the magnetic vector potential has only a z component at these boundaries, therefore, it is equivalent to an infinite bar with uniform current density flowing in the z direction, i.e., a simple two-dimensional situation. The values of A_z are calculated using a 2-D finite element program [18], while A_x and A_y are set to zero. These are then entered in the finite element procedure as boundary conditions on the planes $z = 0$ and $z = z_0$.

RESULTS

The method described above was applied to a steel bar with a slot $\frac{1}{4}$ in deep, $\frac{1}{4}$ in wide, and $\frac{1}{2}$ in long, and the results compared with measured data. The bar was $1\frac{1}{4} \times 1\frac{1}{4}$ in and very long to ensure uniform current distribution in the measurement. Fig. 4 is a block diagram of the experimental setup used to measure flux density profiles. For the finite element modeling a section two inches long was used. The current through the bar for both the experimental setup and the finite element solution was 125 A which resulted in a current density of 124 000 A/m² in the uniform distribution region of the bar. The solution region was divided into 1000 hexahedral isoparametric elements with a total of 1331 nodes and 3993 variables.

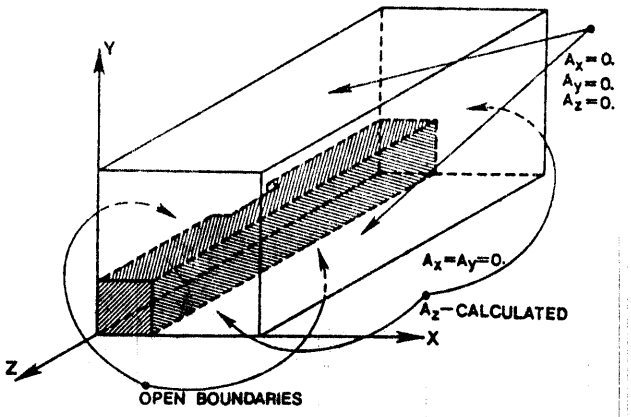

Fig. 3. Boundary conditions.

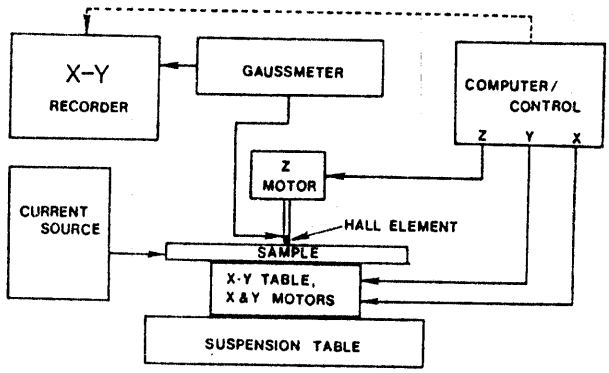

Fig. 4. Experimental setup for leakage field profile measurements.

The solution time for this problem was about $5\frac{1}{2}$ h of CPU time on a VAX 11/780. From the finite element solution of (10) the components of the magnetic vector potential are found at the nodes in the solution region. From the magnetic vector potential, the components of the flux density are calculated using (4). Again, as in the case of current density distribution, the flux density components are assumed to be uniform within an element. These components are calculated at the centroid of the element as a simple average of the nodal flux densities. In order to compare the calculated flux densities with measured values "leakage field profiles" were calculated at cross sectional x-y planes at a lift-off of 0.010 in above the bar surface. Similarly, measurements were taken by scanning the bar with a Hall element at the same lift-off and cross sections as for the calculated profiles. These are compared in Fig. 5 for the normal component (y direction) of the flux density at five different cross sections as indicated in Fig. 5(a). Only a few profiles are actually compared in Fig. 5 because of limitations in the mesh size that can be accommodated on the available computer. These, however, are part of a complete profile of the leakage field of the slot. Using the experimental setup the bar was scanned at short intervals and the Hall element output digitized and displayed (after proper scaling and rotation) to produce a complete three-dimensional leakage field profile as in Fig. 6. The marked curves indicate the individual scans (profiles) corresponding to the calculated leakage profiles in Fig. 5(a).

The numerical results presented in Fig. 5(a) are in good agreement with the experimental measurements. The maxi-

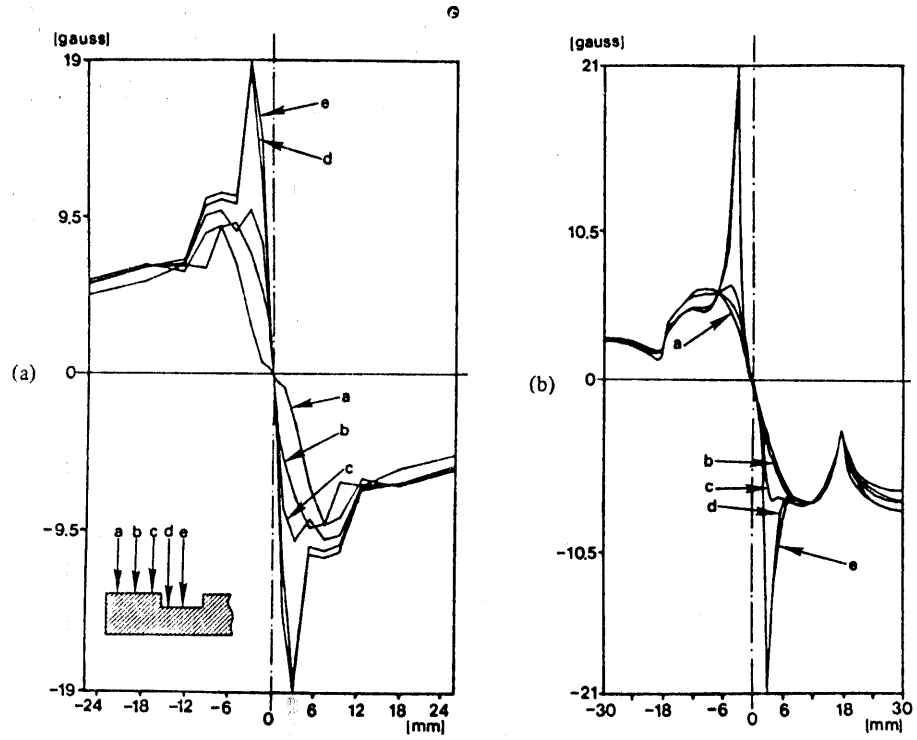

Fig. 5. Comparison of results. (a) Finite element results. (b) Experimental results.

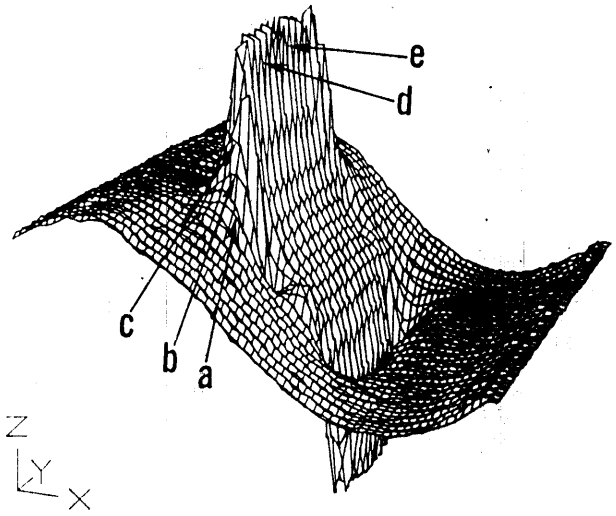

Fig. 6. Three-dimensional leakage field profile of slot. Marked contours correspond to calculated profiles in Fig. 5(a).

mum error in the flux densities is about 9 percent in the slot region. This error is believed to be mainly due to measurement errors, inaccurate machining of the slot and positioning of the Hall probe. This assumption is supported by the fact that the maximum error in the magnetic vector potential compared to a two-dimensional calculation at a cut section through the middle of the slot was only 2.5 percent. Another possible source of error, besides the numerical error is due to partial cancellation of components of the flux density which occur in the calculation process [13].

Conclusion

The method presented here is capable of predicting leakage fields of defects regardless of their shape or location. Important parameters such as variations in conductivities and permeabilities in the vicinity of defects can be incorporated directly. The accuracy of the numerical process is very good considering the relatively coarse discretization and can be improved by mesh refinement. Finite element analysis is developing into a powerful tool for defect characterization capable of providing not only such important information as leakage field profiles for irregular and subsurface defects but also training data from defects and material conditions which are impossible or not practical to manufacture or to measure.

References

[1] A. M. Winslow, "Numerical solution of the quasilinear poisson equation in a nonuniform triangle mesh," *J. Computational Phys.*, vol. 2, pp. 149-172, 1967.

[2] P. Silvester and M. V. K. Chari, "Finite element solution of saturable magnetic field problems," *IEEE Trans. Power App. Syst.*, vol. PAS-89, pp. 1642-1651, 1970.

[3] N. A. Demerdash and T. W. Nehl, "An evaluation of the methods of finite elements and finite differences in the solution of nonlinear electromagnetic fields in electrical machines," *IEEE Trans. Power App. Syst.*, vol. PAS-98, no. 1, pp. 74-87, Jan.-Feb., 1979.

[4] C. W. Trowbridge, "Three-dimensional field computation," *IEEE Trans. Magn.*, vol. MAG-18, no. 1, pp. 293-297, Jan. 1982.

[5] W. Lord and R. Palanisamy, "Development of theoretical models for NDT eddy current phenomena," in *Eddy Current Characterization of Materials and Structures*, ASTM STP 722, G. B. Birnbaum and G. Free, Ed., ASTM, 1981, pp. 5-21.

[6] W. Lord, "A survey of electromagnetic methods of nondestructive testing," in *Mechanics of Nondestructive Testing*, W. W. Stinchcomb, Ed. New York: Plenum, 1980, ch. 3, pp. 77-100.

[7] W. Lord and D. J. Oswald, "Leakage field methods of defect detection," *Int. J. Nondestructive Testing*, vol. 4, pp. 249-274, 1972.

[8] W. Lord and J. H. Hwang, "Finite element modeling of magnetic field/defect interactions," *ASTM J. Testing and Evaluation*, vol. 3, no. 1, pp. 21-25, Jan. 1975.

[9] —, "Defect characterization from magnetic leakage fields," *British J. Nondestructive Testing*, vol. 19, no. 1, pp. 14-18, Jan. 1977.

[10] V. E. Shcherbinin and N. N. Zatsepin, "Calculation of the magnetostatic field of surface defects," *Defektoskopiya*, pp. 59-65, Sep./Oct. 1966.

[11] O. Karlquist, "Calculation of the magnetic field in the ferromagnetic layer of a magnetic drum," *Trans. Royal Institute of Technol.*, no. 86, Stockholm, 1954.

[12] O. C. Zienkiewicz, J. Lyness, and D. R. J. Owen, "Three-dimensional magnetic field determination using a scalar potential–A finite element solution," *IEEE Trans. Magn.*, vol. MAG-13, no. 5, pp. 1649-1656, Sep. 1977.

[13] C. S. Biddlecombe, E. A. Heighway, J. Simkin, and C. W. Trowbridge, "Methods for eddy current computation in three dimensions," *IEEE Trans. Magn.*, vol. MAG-18, no. 2, pp. 492-497, Mar. 1982.

[14] B. M. Irons, "A frontal solution program for finite element analysis," *Int. J. Numerical Methods in Engineering*, vol. 2, pp. 5-32, 1970.

[15] P. Hood, "Frontal solution program for nonsymmetric matrices," *Int. J. Numerical Methods in Engineering*, vol. 10, pp. 379-399, 1976.

[16] S. R. Satish and W. Lord, "Finite element modeling of residual magnetic phenomena," presented at Intermag Conference, Boston, 1980.

[17] J. Weiss and C. M. Stephens, "Finite elements for three-dimensional magnetic fields and its application to turbine generator end region," *IEEE Trans. Power App. Syst.*, vol. PAS-100, no. 4, pp. 1591-1596, Apr. 1981.

[18] R. Palanisamy and W. Lord, "Finite element modeling of electromagnetic NDT phenomena," *IEEE Trans. Magn.*, vol. MAG-15, no. 6, pp. 1479-1481, Nov. 1979.